AGU PUBLICATIONS

Geophysical Research Letters

RESEARCH LETTER
10.1002/2014GL060914

Key Points:
- Regionally specific models of flow beneath subducting slabs are presented
- Subslab dynamics controlled by deflection of mantle flow in vicinity of slab
- Predicted finite strain directions generally agree with anisotropy observations

Supporting Information:
- Readme
- Table S1
- Text S1
- Movie S1
- Movie S2
- Movie S3
- Movie S4
- Figure S1
- Figure S2
- Figure S3
- Figure S4
- Figure S5
- Figure S6
- Figure S7
- Figure S8
- Figure S9

Correspondence to:
K. Paczkowski,
karen.paczkowski@gmail.com

Citation:
Paczkowski, K., C. J. Thissen, M. D. Long, and L. G. J. Montési (2014), Deflection of mantle flow beneath subducting slabs and the origin of subslab anisotropy, *Geophys. Res. Lett.*, *41*, doi:10.1002/2014GL060914.

Received 15 JUN 2014
Accepted 15 SEP 2014
Accepted article online 16 SEP 2014

Deflection of mantle flow beneath subducting slabs and the origin of subslab anisotropy

Karen Paczkowski[1,2], Christopher J. Thissen[2], Maureen D. Long[2], and Laurent G. J. Montési[1]

[1]Department of Geology, University of Maryland, College Park, Maryland, USA, [2]Department of Geology and Geophysics, Yale University, New Haven, Connecticut, USA

Abstract Global compilations of subslab shear wave splitting parameters show a mix of trench-parallel and trench-perpendicular fast directions that often directly contradict predictions from two-dimensional models of slab-entrained flow. Here we show that subslab anisotropy is consistent with three-dimensional geodynamic models that feature the interaction between subducting slabs and regional mantle flow. Each model represents a specific region for which high-quality source-side shear wave splitting data are available. We compare the distribution of finite strain in the models with shear wave splitting observations, showing that both trench-parallel and trench-perpendicular fast directions can be explained by deflection of regional mantle flow around or beneath subducted slabs. Subslab maximum elongation directions calculated from our models depend on a combination of geometry factors (such as slab dip angle and maximum depth), mechanical parameters (such as decoupling between the slab and the subjacent mantle), and the orientation and magnitude of the regional mantle flow.

1. Introduction

Measurements of seismic anisotropy provide powerful observational constraints on dynamic processes in the Earth's mantle, as there is a relationship between the strain induced by mantle flow and the resulting seismic anisotropy [e.g., *Long and Becker*, 2010]. Observations of anisotropy in subduction zones worldwide, primarily from studies of shear wave splitting, have yielded a rich variety of splitting behavior [e.g., *Long*, 2013]. However, measurements of splitting due to anisotropy in the upper mantle beneath slabs (subslab anisotropy) have proven particularly puzzling to interpret in terms of mantle flow; many subduction systems exhibit fast splitting directions that are subparallel to the trench, contradicting the predictions of the simplest flow models. A variety of conceptual models that consider three-dimensional subslab flow [e.g., *Russo and Silver*, 1994; *Long and Silver*, 2008], slab deformation [*Di Leo et al.*, 2014], or the presence of a tilted, subducted oceanic asthenosphere layer with a strong radial anisotropy component [*Song and Kawakatsu*, 2012] have been proposed to explain observed patterns of fast splitting directions in the subslab mantle.

Recent progress has been made in modeling investigations of the three-dimensional pattern of mantle flow in subduction systems, from both a numerical [e.g., *Faccenda and Capitanio*, 2012, 2013; *Di Leo et al.*, 2014; *Li et al.*, 2014; *Rodríguez-González et al.*, 2014] and laboratory [e.g., *Druken et al.*, 2011] point of view. Although these studies consider trench migration and the complex shape of slabs, they do not consider that subduction zones exist within a global mantle flow field [e.g., *Conrad and Behn*, 2010]. Interaction between subduction-induced mantle flow, the global mantle flow, and trench migration affects subslab mantle flow [*Paczkowski et al.*, 2014] and potentially the development of anisotropy in the subslab mantle. Here we discuss the finite strain field that develops in instantaneous three-dimensional kinematic-dynamic models of individual subduction systems that include global mantle flow, plate kinematics, and slab geometry parameters. The distribution of finite strain in the subslab mantle predicted by each of our models provides an approximation to seismic anisotropy that can be compared with high-quality source-side shear wave splitting measurements that sample the subslab mantle. Our models demonstrate that most observations of subslab splitting globally can be explained as a consequence of strain in a subslab mantle flow field that results from the interaction between slabs and the regional mantle flow field.

2. Numerical Modeling Approach

In order to facilitate comparison between subslab anisotropy observations and numerical model predictions, we only model subduction systems for which uniformly processed, high-quality source-side shear wave

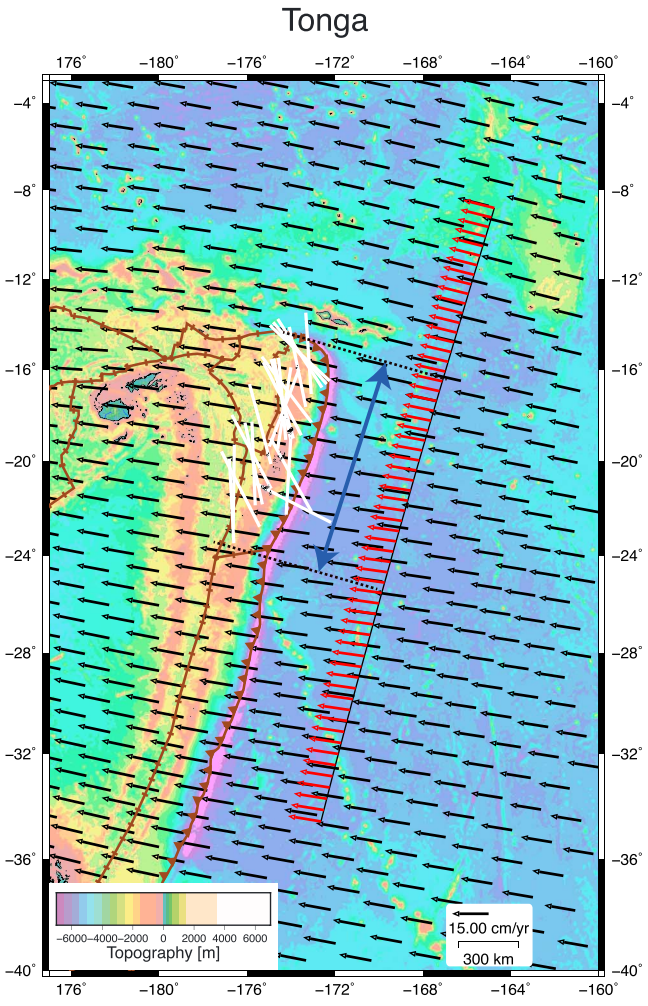

Figure 1. Mantle flow and splitting observations for the Tonga subduction zone. Bathymetry (color field) and vertically averaged horizontal velocity in the upper mantle (black arrows) predicted for the Tonga subduction zone, where the Pacific Plate subducts to the west beneath the Australia Plate. Individual source-side shear wave splitting measurements for the subslab mantle (white) [*Foley and Long*, 2011] are available for a segment of the boundary of length L_{trench} (blue double-ended arrows). The global mantle flow [*Conrad and Behn*, 2010], depth-averaged over the upper mantle, is expressed in a reference frame fixed with the trench (black arrows) and average along a trench-parallel transect (red arrows) to provide an estimate of the regional flow field. Plate boundaries are indicated in brown [*Bird*, 2003]. Similar figures for each subduction zone segment used here are available in the supporting information.

splitting measurements are available. We used measurements from several recent studies [*Foley and Long*, 2011; *Lynner and Long*, 2013, 2014] that directly constrain anisotropy in the subslab mantle beneath the Tonga, Caribbean, Scotia, Alaska, Aleutians, Central America, Kuril, North Honshu, Izu-Bonin, Ryukyu, and Sumatra subduction zones. For each of these subduction zone segments, we have compiled values for slab dip (α_s), maximum slab penetration depth (D_{slab}), and estimates of trench-fixed regional mantle flow velocity scaled by the convergence velocity ($\overline{V}$) and azimuth (θ_v) that combine a global mantle flow model [*Conrad and Behn*, 2010] and observed plate motions and trench migration rates [*Schellart et al.*, 2008]. The dips (α_s) and depths (D_{slab}) of slabs in the upper mantle (Table S1 in the supporting information) are taken from a single global compilation [*Lallemand et al.*, 2005] wherever possible (further details are contained in the supporting information). These estimates are derived from global mantle tomography models and necessarily involve a degree of subjectivity [*Lallemand et al.*, 2005].

The regional mantle flow results from global mantle flow, plate motion, and trench migration [*Paczkowski et al.*, 2014]. Therefore, our modeling approach requires estimates of these quantities for each region under study. Global mantle flow was estimated using a global mantle circulation model [*Conrad and Behn*, 2010], which combines the effects of density-driven and plate-driven flow in the mantle. We calculated the vertically averaged horizontal upper mantle flow velocities from *Conrad and Behn* [2010] in a no-net-rotation (NNR) reference frame near each subduction segment (Figure 1). Trench migration velocities for each segment were expressed in the NNR reference frame by combining the estimates of *Schellart et al.* [2008] of trench-perpendicular trench migration velocity (rollback or advance) and the trench-parallel component of downdip slab motion [*DeMets et al.*, 1994] to represent the trench-parallel component of trench migration. Subtracting the trench migration velocity from the depth-averaged global mantle flow field provides an estimate of the global mantle flow near each trench in a local trench-fixed reference frame. Finally, we define the regional mantle flow (Table S1) as the local trench-fixed global flow field averaged along a transect that roughly corresponds to the back wall of our model. Full details of these calculations can be found in the supporting information.

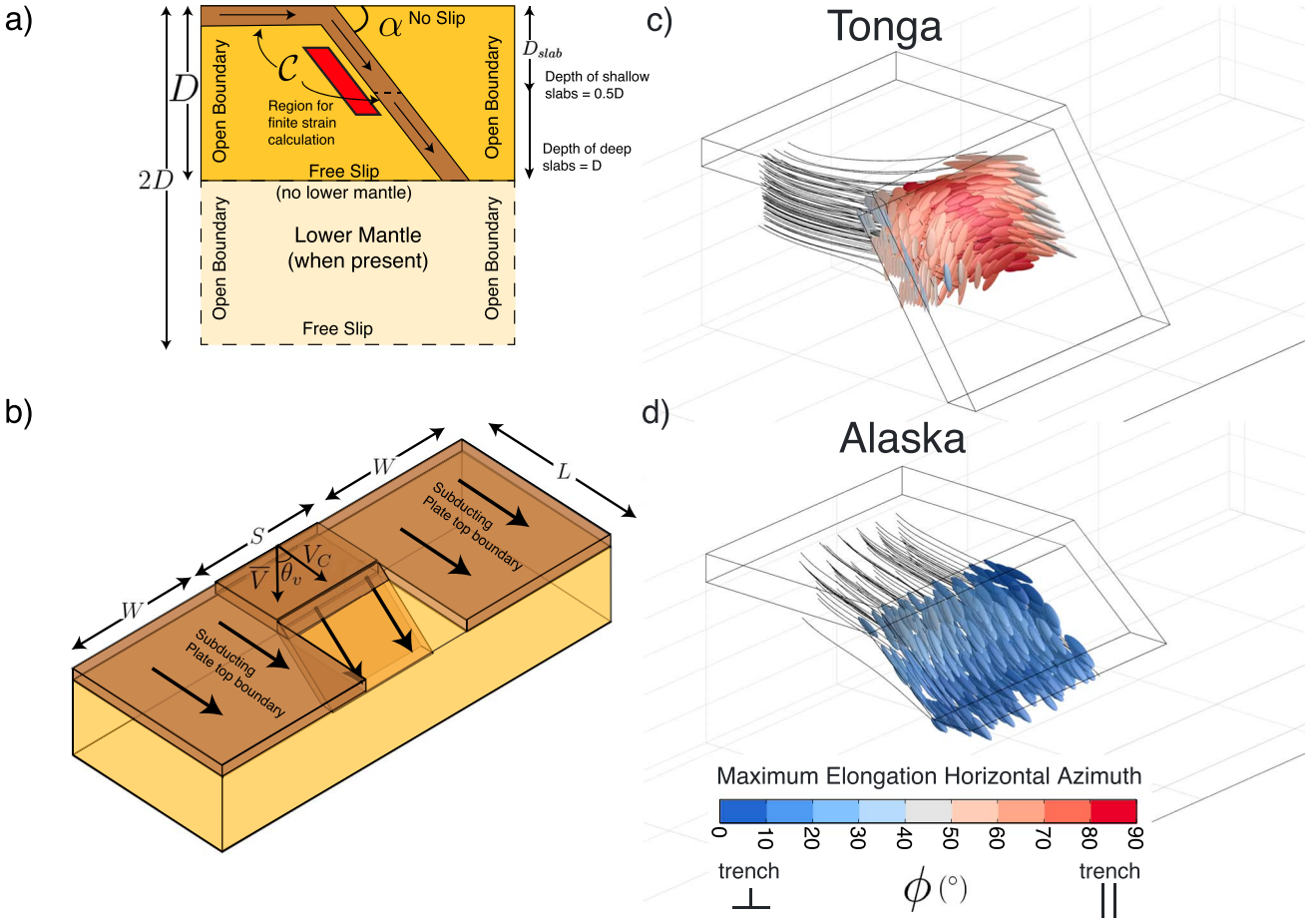

Figure 2. Schematic model setup and results for two subduction zones. (a) Side-view schematic diagram of the basic model setup, with the subducting plate in brown. The dip, α_s, and depth, D_{slab}, of the subducting plate, the coupling factor between the subducting plate and the underlying mantle, C, the depth of the upper mantle and lower mantle (when present), D, and the boundary conditions are shown. The region where finite strain ellipsoids are calculated is shown in red and corresponds to the region sampled by source-side shear wave splitting observations [*Foley and Long*, 2011]. (b) Perspective view of the model geometry. The arrows indicate plate motion, the convergence velocity V_c and the background mantle flow (magnitude scaled by the convergence velocity $\overline{V}$ and azimuth θ_v positive clockwise from the convergence direction). (c) Finite strain ellipsoids and streamlines (black lines) for a fully decoupled model representing the Tonga subduction zone. The finite strain ellipsoids are colored by the horizontal azimuth of the maximum elongation direction and show dominantly trench-parallel maximum elongation directions as the background mantle flow is directed around the edges of the slab. (d) Same as Figure 2c but for the Alaska subduction zone. The finite strain ellipsoids show dominantly trench-perpendicular maximum elongation directions as the background mantle flow is deflected underneath the short Alaska slab. Videos of finite strain development for Figures 2c and 2d are available in the supporting information.

For each subduction zone, we constructed a three-dimensional model of the subslab mantle flow field for the geometry and geodynamic parameters appropriate for each subduction zone (Table S1). In these models, mantle flow is driven by the motion of a planar subducting slab and a mantle pressure gradient applied to the upper mantle (Figure 2a). We constructed these steady state, three-dimensional, kinematically driven mantle flow models, assuming an incompressible, isoviscous, Newtonian fluid, using the COMSOL Multiphysics® finite element modeling software, which has been shown to have excellent performance for subduction zone modeling [*van Keken et al.*, 2008]. The density is set to the low value of 10^{-20} kg/m^3 to minimize the effects of inertia, and the effects of thermal buoyancy and gravity are ignored. The slab width, S, is set to $1.5D$, where D is the thickness of the upper mantle (~670 km). The edges of the model are located a distance $W = 2.5D$ from the edges of the subducting slab. The width of the model in the subduction direction, L, is set to $D\cot(\alpha_s) + 2.2D$ and depends on the dip of the subducting plate α_s. L and W are chosen to minimize any effect of the model boundaries. In some models the lower mantle is included as a layer of thickness D of a Newtonian material that has 30 times the viscosity of the upper mantle [*Čížková et al.*, 2012].

The model is meshed with free tetrahedra in two steps. First, the wedge and subslab domains are meshed at high resolution (element size between 0.05*D* to 0.1*D*). Then, the mesh in the surrounding mantle edges and the lower mantle is generated by matching the subslab and wedge meshes at the boundaries, but with progressively coarser elements away from the slab. Free slip is imposed on the bottom model boundary at a depth of 1340 km or, when no lower mantle is included, at a depth of 670 km (the base of the transition zone). The top surface of the model at the base of the overriding plate is fixed with a no-slip boundary condition as appropriate for the trench-fixed reference frame of our calculations. The subducting plate and the downgoing slab are moving at the trench-perpendicular convergence velocity V_c.

Coupling between the slab and the surrounding mantle is implemented with the help of a coupling factor C such that the velocity imposed on the mantle in contact with the slab and the subducting plate is CV_c. The interface between the slab and the overlying mantle wedge transitions from fully decoupled ($C = 0$) at depths shallower than 80 km to fully coupled ($C = 1$) below 80 km [*Wada and Wang*, 2009]. The coupling factor is uniform along the interface between the subducting slab and the mantle beneath it. The effect of changing the subslab coupling factor has been explored systematically in our models. (In contrast to our modeling approach, *Conrad and Behn* [2010] effectively assume full coupling between slabs and the subslab mantle when considering global density-driven flow; the implications of this are discussed in the supporting information.)

Our models feature a background mantle flow that represents global mantle flow and trench migration. In our local trench-fixed reference frame, a subduction system with strong trench rollback corresponds to a model with a strong background flow field coming from the back-arc side. The background flow is generated by imposing on the model sides a pressure field that varies linearly with horizontal distance. The magnitude $\overline{V}$ and azimuth $\theta_{v,}$ (counted positive clockwise from the convergence direction) of the background flow are calculated a posteriori by averaging the model mantle velocity along the upper mantle section of the wall behind the subducting slab [*Paczkowski et al*., 2014]. For each subduction zone segment of interest, the magnitude and azimuth of the pressure gradient are iterated until the background flow field in the model matches the regional mantle flow field evaluated from global convection models and observed trench migration rate, as described above.

3. Finite Strain Calculations

Our models are evaluated by comparing finite strain ellipsoids (FSEs) in our models with observations of subslab seismic anisotropy. The anisotropy data set is limited to source-side shear wave splitting measurements [*Lynner and Long*, 2013], thus avoiding complications due to complex anisotropy in the mantle wedge. Histograms of the observed seismic fast directions for each subduction zone segment are shown in Figure 3.

We calculated finite strain ellipsoids (FSEs) by integrating the velocity gradient field along particle streamlines [*McKenzie*, 1979] using a fifth-order Runge-Kutta integration method with adaptive step size [*Press et al*., 2007]. The orientation of the maximum elongation of the FSEs can be used as a proxy for the geometry of anisotropy [*Ribe*, 1992; *Becker et al*., 2003; *Lev and Hager*, 2008] for most olivine lattice preferred orientation scenarios [*Karato et al*., 2008; *Long and Becker*, 2010]. As the FSE may not always align with the local mantle flow trajectory [e.g., *Li et al*., 2014], this approach improves on our previous work, which only considered mantle flow, not strain [*Paczkowski et al*., 2014]. The effects of inherited fabrics, which may be significant [e.g., *Skemer et al*., 2012], are ignored here, but our approach should be a good approximation for regions with relatively large amounts of accumulated strain (stretch ratios greater than ~3).

We examine the FSEs in a volume corresponding to the subslab region sampled by source-side shear wave splitting measurements [*Foley and Long*, 2011] (160 km to 435 km depth, approximately 200 km to 67 km behind the slab and 670 km along the strike of the slab; Figure 2a) and containing 1331 FSEs. Further details of these calculations, along with videos showing the accumulation of finite strain along particle streamlines for several example models, can be found in the supporting information.

The horizontal projection of maximum elongation directions of the finite strain ellipsoids were compared with the fast directions obtained from source-side shear wave splitting. To facilitate the comparison, both data sets are converted to probability density functions by smoothing with a Gaussian kernel using a Gaussian optimal bandwidth [*Bowman and Azzalini*, 1997], as shown in Figure 3.

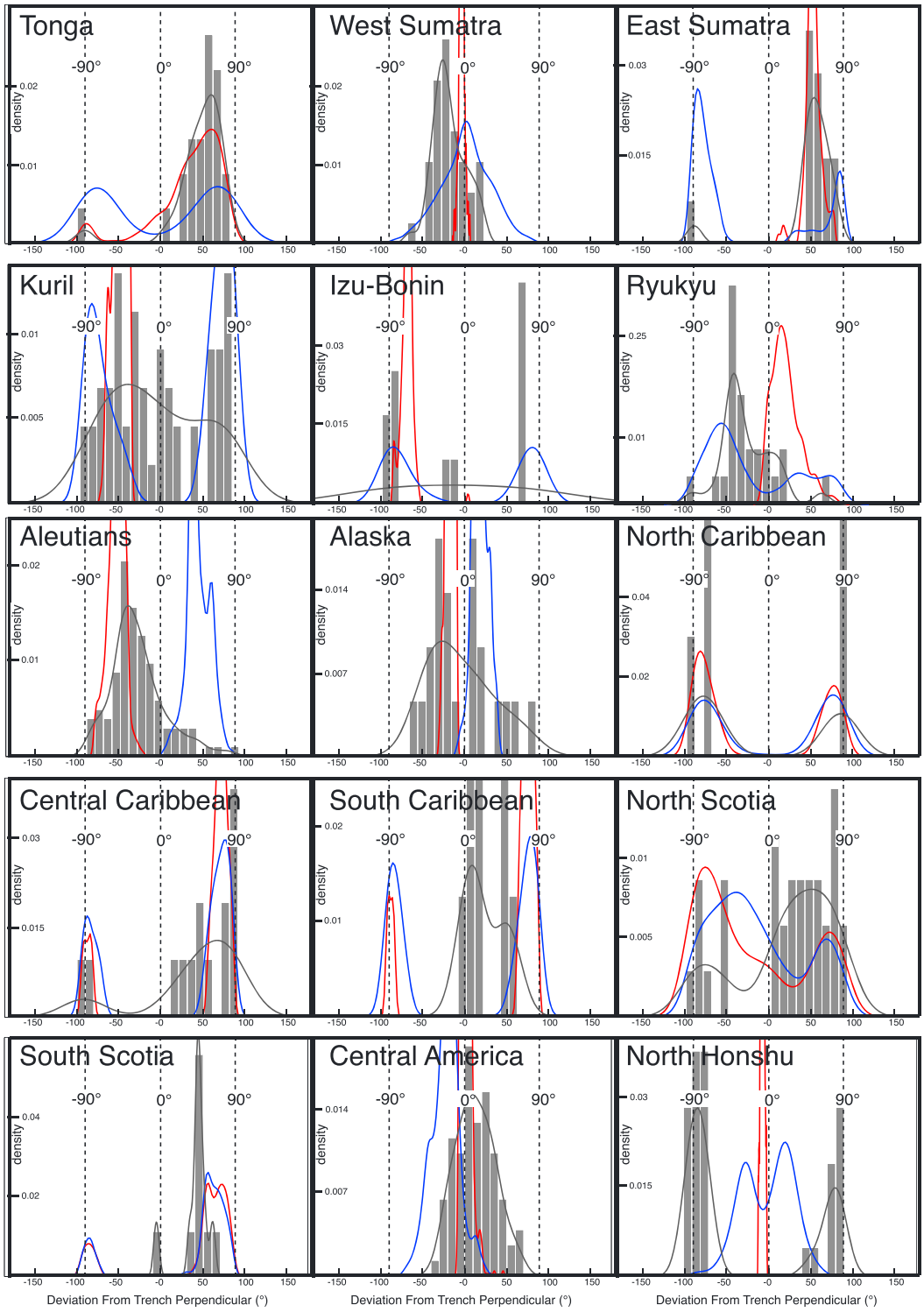

Figure 3

4. Results

Figure 2c illustrates the generation of FSEs elongated parallel to the trench in the subslab domain of a model that represents the Tonga subduction zone, which exhibits a well-defined pattern of trench-parallel fast splitting directions [*Foley and Long*, 2011]. Tonga has a steeply dipping, deep slab ($\alpha_s = 56°$, $D_{slab} = 670$ km) and rapid trench rollback [*Schellart et al*., 2008]. Accordingly, the background mantle flow enters the model domain flowing in a trench-perpendicular direction ($\overline{V} = 1.76V_c$, $\theta_v = -7°$) but is abruptly deflected in a trench-parallel direction by the slab. The slab acts as an obstruction and directs mantle flow toward escape paths around the slab edge [*Paczkowski et al*., 2014].

The FSEs associated with this flow field are elongated in a trench-parallel direction (Figures 2c and 3) in the region sampled by source-side shear wave splitting measurements (Figure 2a), even though the background mantle flow is trench perpendicular (Figure 1). A model with full coupling also shows dominantly trench-parallel maximum elongation directions, although slightly less than for the decoupled model (Figure 3). The FSE maximum elongation horizontal azimuths show good agreement with shear wave spilling observations, especially for the coupled model (Figure 3), suggesting that the approximately trench-parallel seismic anisotropy directions beneath Tonga may result from the deflection of the regional mantle flow field around the slab.

Figure 2d illustrates the generation of FSEs elongated perpendicular to the trench in the subslab domain of a model that represents the Alaska subduction zone, which has a relatively moderately dipping, short slab ($\alpha_s = 40°$, $D_{slab} = 300$ km). The background mantle flow enters the model domain flowing in a trench-perpendicular direction ($\overline{V} = 0.49V_c$, $\theta_v = 17°$). The slab again acts as an obstruction to the background mantle flow, but with this subduction zone geometry, the flow is deflected underneath the slab and its azimuth remains largely unchanged [*Paczkowski et al*., 2014]. The maximum elongation directions of the FSEs, unlike the Tonga model, are dominantly trench perpendicular through the region for both fully decoupled and fully coupled models, in agreement with observations of subslab seismic anisotropy (Figure 3 and the supporting information). This suggests deflection of mantle flow is also a plausible geodynamic explanation for trench-perpendicular fast directions in the subslab mantle, as observed in the Alaska subduction zone.

We have developed similar regional geodynamic models for each of the subduction zone segments in the source-side shear wave splitting database (Table S1). The results of each subduction zone model are summarized, and the distribution of FSE maximum elongation horizontal azimuths is compared to the measured fast splitting directions in Figure 3. We include results for both fully decoupled and fully coupled models. With the exception of the model representing the Aleutians subduction zone, the amount of coupling has relatively minor effects on the distribution of maximum elongation azimuths. The effect of including a lower mantle in our model is minimal (supporting information) [see also *Paczkowski et al*., 2014]. In general, this comparison demonstrates that in most subduction systems, observations of subslab anisotropy can be explained by the interactions among subducting slabs, plate motions, trench migration, and global mantle flow, as discussed further below.

5. Discussion

Our analysis reveals that the orientation of the mantle flow deflection and the resulting maximum elongation directions are highly sensitive to subduction zone geometry, the direction and magnitude of the regional mantle flow in a trench-fixed reference frame, and (in some cases) the coupling between the subducting plate and the underlying mantle. A more systematic study that investigates the effect of different model parameters on subslab mantle flow (although not FSEs) is described in *Paczkowski et al*. [2014].

Figure 3. Numerical model predictions and seismic anisotropy observations. Distributions of horizontal azimuth of the maximum elongation directions and the seismic anisotropy fast direction are shown for each subduction zone segment (0° is trench perpendicular and ± 90° is trench parallel). The horizontal projection of the maximum elongation directions of the finite strain ellipsoids is shown for both fully coupled models (red lines) and fully decoupled models (blue lines). Models include a viscous lower mantle with a Newtonian viscosity 30 times greater than the viscosity of the upper mantle. The distribution of seismic anisotropy fast directions for the subduction zone of interest are shown as both probability density (grey lines) and as the histogram of raw data, binned in 10° intervals, and normalized to unit mass (grey bars). Seismic anisotropy directions are shown as deviations from the trench-perpendicular direction, defined as perpendicular to the transect used to calculate the regional mantle flow (supporting information).

Finite strain accumulates gradually throughout the subslab mantle in our models, reaching the largest magnitudes close to the slab (see Movies S1–S4 and Figures S6–S9 in the supporting information). For fully decoupled long slabs where flow is deflected around the slab edges, the maximum elongation directions also develop trench-parallel directions consistently throughout the subslab mantle. For fully coupled long slabs, however, a component of trench-perpendicular maximum elongations develops just beneath the slab (Figures 3, S6, and S7), which increases the width of the distribution of FSE azimuths. In contrast, for short slabs where the regional mantle flow is deflected beneath the slab, trench-perpendicular maximum elongation directions accumulate gradually for both fully decoupled and fully coupled cases (Figures 3, S8, and S9).

The finite strain patterns we predict are generally similar to those found by fully dynamic models of subduction with a retreating trench [*Faccenda and Capitanio*, 2012, 2013; *Li et al*., 2014], which confirms the validity of our approach of including slab retreat as part of a regional mantle flow. These studies found that subslab shear wave splitting should generally be influenced by both entrained flow directly beneath the plate and deeper toroidal flow due to trench retreat. Our study explicitly explores how slab geometry, trench migration, and global mantle flow interact to produce such variable finite strain patterns.

The maximum elongation directions of the FSEs predicted by our models generally agree well with source-side shear wave splitting fast directions for many of the subduction zones examined in this study. This suggests that the regional mantle flow and its interaction with slab-entrained flow are captured adequately in our models and that this interaction provides a plausible explanation for both trench-parallel and trench-perpendicular shear wave splitting directions. In systems with a trench-parallel regional mantle flow field (e.g., Izu-Bonin), this flow continues unaltered through the subslab domain and produces trench-parallel maximum elongation directions, even with a relatively high coupling factor. For deep, steeply dipping slabs (e.g., Tonga, East Sumatra, Kuril, Scotia, and Caribbean), an originally trench-perpendicular regional mantle flow is deflected around the slab edges, creating trench-parallel maximum elongation directions in the subslab mantle. Subduction zones with deep, steeply dipping slabs but that exhibit primarily trench-perpendicular fast splitting directions may be explained by partial coupling between the subducting slab and the subjacent mantle that entrains trench-perpendicular flow (Ryukyu) or by weak regional mantle flow field magnitudes relative to the convergence velocity (West Sumatra). For subduction zones with shallow slabs (e.g., Aleutian, Alaska, and Central America), trench-perpendicular regional mantle flow fields are deflected beneath the slab, preserving the original regional mantle flow direction and creating trench-perpendicular maximum elongation directions.

The model comparisons are less satisfactory for three of our fifteen cases: the Kuril, North Honshu, and South Caribbean subduction zones. All three cases include complexity in their tectonic setting that is not captured by our relatively simple models. The seismic anisotropy fast directions for the Kuril subduction zone transition from primarily trench perpendicular to primarily trench parallel along the length of the trench, whereas the FSE are consistently trench parallel or at 45° from the trench direction, depending on the degree of coupling. It may be that the degree of coupling between the slab and the subjacent mantle changes along the strike of the subduction zone in relation to lithospheric age [*Lynner and Long*, 2014]. The global mantle flow field near the North Honshu subduction zone has variable direction and low magnitude, which suggests that the fairly uniform background mantle flow present in the models may not accurately represent the ambient conditions for this subduction zone. Improved models with spatially variable background mantle flow may agree more completely with the seismic anisotropy observations from that region. Seismic data from the South Caribbean subduction zone are principally derived from events located close to the thick continental lithosphere of South America, which may influence the subslab anisotropy in a way not captured by our model [*Miller and Becker*, 2012; *Lynner and Long*, 2013].

Perhaps the most poorly constrained parameter in our models is the degree of coupling between the subducting slab and the underlying subslab mantle, as other subduction zone parameters and regional mantle flow can be estimated independently of regional shear wave splitting measurements. In many subduction zones (Tonga, West Sumatra, Izu-Bonin, Alaska, North Caribbean, Central Caribbean, South Caribbean, North Scotia, South Scotia, Central America, and North Honshu), subslab maximum elongation directions (and thus splitting directions) are largely insensitive to the coupling factor and are instead controlled by slab geometry and kinematics. Seismic observations of fast directions at subduction zones in

which subslab maximum elongation directions are sensitive to the coupling factor suggest nearly full coupling in some cases (East Sumatra and Aleutians) and partial coupling (Ryukyu) or spatially variable coupling (Kuril) [*Lynner and Long*, 2014] in other cases. When the slab and mantle are well coupled, a boundary layer of entrained mantle flow develops beneath the slab [*Paczkowski et al*., 2014], favoring trench-perpendicular maximum elongation directions.

Physically, partial coupling may result from a thin layer of low-viscosity material, such as a layer of entrained buoyant, weak asthenosphere [*Phipps Morgan et al*., 2007; *Long and Silver*, 2009], partial melt [*Kohlstedt*, 2002; *Katz et al*., 2006; *Kawakatsu et al*., 2009; *Schmerr*, 2012], or solidified wet gabbro [*Karato*, 2012], and may be facilitated by shear heating [*Larsen et al*., 1995; *Long and Silver*, 2009] or the onset of small-scale convection [*Lynner and Long*, 2014]. Alternatively, a non-Newtonian rheology may also thin the mechanical boundary layer at the base of the slab and partially decouple the slab and the subjacent mantle [*Parmentier et al*., 1976; *Tovish et al*., 1978; *McKenzie*, 1979; *Faccenda and Capitanio*, 2013]. While our models cannot discriminate among these different scenarios, some level of decoupling appears necessary for the Ryukyu and Kuril subduction zones, whereas the Tonga and East Sumatra subduction zones are better explained by fully coupled models. Improved constraints on the level of coupling in each location may shed new light on the nature of the oceanic lithosphere-asthenosphere boundary and its relation to the geologic history of oceanic plates. Furthermore, our results suggest that global circulation models may need to be revisited by including very high viscosity, potentially rigid slabs that are only partially coupled with the subjacent mantle.

6. Summary

We developed a suite of instantaneous three-dimensional kinematic-dynamic models of individual subduction systems that consider the interaction between slab geometry and a regional mantle flow that represents a combination of global mantle flow, trench migration, and plate motion. In these experiments, the subducting slab acts as a barrier that deflects regional mantle flow either around or beneath the slab. Deflections around the sides of deep slabs create trench-parallel maximum elongation directions behind the slab. Deflections beneath shorter slabs preserve the regional mantle flow direction, making it possible to have trench-perpendicular maximum elongation directions in the subslab mantle. In some cases, coupling between the subducting slab and the underlying mantle influences the maximum elongation directions, with coupling producing more trench-perpendicular directions. Comparisons between the horizontal azimuth of the maximum elongations and the orientations of source-side shear wave splitting fast directions for specific subduction zones are generally successful. Including complexities in the regional flow field, the degree of coupling, and/or the presence of continental lithosphere may further improve the agreement between models and seismic observations. Nevertheless, the models shown here suggest that deflection of regional mantle flow is a geodynamically plausible explanation for the global distribution of subslab seismic anisotropy directions.

Acknowledgments

Data supporting Figure 3 can be found in *Foley and Long* [2011] and *Lynner and Long* [2013, 2014].We are grateful to Clint Conrad, Dave Bercovici, Shun Karato, Mark Brandon, Chris Kincaid, and Colton Lynner for discussions and comments. This work was funded by NSF grants EAR-0911286 (M.D.L.), EAR-0911151, and OCE-1060878 (L.G.J.M. and K.P.). M.D.L. acknowledges additional support from an Alfred P. Sloan Research Fellowship, and C.J.T. acknowledges support from an NSF Graduate Research Fellowship under grant DGE-1122492. We thank two anonymous reviewers and the Editor for their constructive and helpful reviews and for challenging us to improve this paper.

Michael Wysession thanks two anonymous reviewers for their assistance in evaluating this paper.

References

Becker, T. W., J. B. Kellogg, G. Ekström, and R. J. O'Connell (2003), Comparison of azimuthal seismic anisotropy from surface waves and finite strain from global mantle-circulation models, *Geophys. J. Int.*, *155*, 696–714.

Bird, P. (2003), An updated digital model of plate boundaries, *Geochem. Geophys. Geosyst.*, *4*(3), 1027, doi:10.1029/2001GC000252.

Bowman, A. W., and A. Azzalini (1997), *Applied Smoothing Techniques for Data Analysis: The Kernel Approach With S-Plus Illustrations*, Oxford Univ. Press, New York.

Čížková, H., A. P. van den Berg, W. Spakman, and C. Matyska (2012), The viscosity of Earth's lower mantle inferred from sinking speed of subducted lithosphere, *Phys. Earth Planet. Inter.*, *200*, 56–62, doi:10.1016/j.pepi.2012.02.010.

Conrad, C. P., and M. D. Behn (2010), Constraints on lithosphere net rotation and asthenospheric viscosity from global mantle flow models and seismic anisotropy, *Geochem. Geophys. Geosyst.*, *11*, Q05W05, doi:10.1029/2009GC002970.

DeMets, C., R. G. Gordon, D. F. Argus, and S. Stein (1994), Effect of recent revisions to the geomagnetic reversal time scale on estimates of current plate motions, *Geophys. Res. Lett.*, *21*, 2191–2194.

Di Leo, J., A. Walker, Z.-H. Li, J. Wookey, N. Ribe, J.-M. Kendall, and A. Tommasi (2014), Development of texture and seismic anisotropy during the onset of subduction, *Geochem. Geophys. Geosyst.*, *15*, 192–212, doi:10.1002/2013GC005032.

Druken, K., M. Long, and C. Kincaid (2011), Patterns in seismic anisotropy driven by rollback subduction beneath the High Lava Plains, *Geophys. Res. Lett.*, *38*, L13310, doi:10.1029/2011GL047541.

Faccenda, M., and F. A. Capitanio (2012), Development of mantle seismic anisotropy during subduction-induced 3-D flow, *Geophys. Res. Lett.*, *39*, L11305, doi:10.1029/2012GL051988.

Faccenda, M., and F. A. Capitanio (2013), Seismic anisotropy around subduction zones: Insights from three-dimensional modeling of upper mantle deformation and SKS splitting calculations, *Geochem. Geophys. Geosyst.*, *14*, 243–262, doi:10.1002/ggge.20055.

Foley, B. J., and M. D. Long (2011), Upper and mid-mantle anisotropy beneath the Tonga slab, *Geophys. Res. Lett.*, *38*, L02303, doi:10.1029/2010GL046021.
Karato, S. (2012), On the origin of the asthenosphere, *Earth Planet. Sci. Lett.*, *321-322*, 95–103.
Karato, S.-I., H. Jung, I. Katayama, and P. Skemer (2008), Geodynamic significance of seismic anisotropy of the upper mantle: New insights from laboratory studies, *Annu. Rev. Earth Planet. Sci.*, *36*, 59–95, doi:10.1146/annurev.earth.36.031207.124120.
Katz, R. F., M. Spiegelman, and B. Holtzman (2006), The dynamics of melt and shear localization in partially molten aggregates, *Nature*, *442*, 676–679, doi:10.1038/nature05039.
Kawakatsu, H., P. Kumar, Y. Takei, M. Shinohara, T. Kanazawa, E. Araki, and K. Suyehiro (2009), Seismic evidence for sharp lithosphere-asthenosphere boundaries of oceanic plates, *Science*, *324*, 499–502, doi:10.1126/science.1169499.
Kohlstedt, D. L. (2002), Partial melting and deformation, in *Plastic Deformation in Minerals and Rocks, 51*, pp. 105–125, Mineralog. Soc. Am., Washington, D. C.
Lallemand, S., A. Heuret, and D. Boutelier (2005), On the relationships between slab dip, back-arc stress, upper plate absolute motion, and crustal nature in subduction zones, *Geochem. Geophys. Geosyst.*, *6*, Q09006, doi:10.1029/2005GC000917.
Larsen, T. B., D. A. Yuen, and A. V. Malevsky (1995), Dynamical consequences on fast subducting slabs from a self-regulating mechanism due to viscous heating in variable viscosity convection, *Geophys. Res. Lett.*, *22*(10), 1277–1280, doi:10.1029/95GL01112.
Lev, E., and B. H. Hager (2008), Prediction of anisotropy from flow models: A comparison of three methods, *Geochem. Geophys. Geosyst.*, *9*, Q07014, doi:10.1209/2008GC002032.
Li, Z. H., J. F. Di Leo, and N. M. Ribe (2014), Subduction-induced mantle flow, finite strain, and seismic anisotropy: Numerical modeling, *J. Geophys. Res. Solid Earth*, *119*, 5052–5076, doi:10.1002/2014JB010996.
Long, M. D. (2013), Constraints on subduction geodynamics from seismic anisotropy, *Rev. Geophys.*, *51*, 76–112, doi:10.1002/rog.20008.
Long, M. D., and T. W. Becker (2010), Mantle dynamics and seismic anisotropy, *Earth Planet. Sci. Lett.*, *297*, 341–354, doi:10.1016/j.epsl.2010.06.036.
Long, M. D., and P. G. Silver (2008), The subduction zone flow field from seismic anisotropy: A global view, *Science*, *318*, 315–318, doi:10.1126/science.1150809.
Long, M. D., and P. G. Silver (2009), Mantle flow in subduction systems: The subslab flow field and implications for mantle dynamics, *J. Geophys. Res.*, *114*, B10312, doi:10.1029/2008JB006200.
Lynner, C., and M. D. Long (2013), Sub-slab seismic anisotropy and mantle flow beneath the Caribbean and Scotia subduction zones: Effects of slab morphology and kinematics, *Earth Planet. Sci. Lett.*, *361*, 367–378, doi:10.1016/j.epsl.2012.11.007.
Lynner, C., and M. D. Long (2014), Sub-slab seismic anisotropy beneath the Sumatra and circum-Pacific subduction zones from source-side shear wave splitting observations, *Geochem. Geophys. Geosyst.*, *15*, 2262–2281, doi:10.1002/2014GC005239.
McKenzie, D. (1979), Finite deformation during fluid flow, *Geophys. J. Roy. Astron. Soc.*, *58*, 689–715.
Miller, M. S., and T. W. Becker (2012), Mantle flow deflected by interactions between subducted slabs and cratonic keels, *Nat. Geosci.*, *5*, 726–730, doi:10.1038/ngeo1553.
Paczkowski, K., L. G. J. Montési, M. D. Long, and C. J. Thissen (2014), Three-dimensional flow in the sub-slab mantle, *Geochem. Geophys. Geosyst.*, doi:10.1002/2014GC005441.
Parmentier, E. M., D. L. Turcotte, and K. E. Torrance (1976), Studies of finite amplitude non-Newtonian thermal convection with application to convection in the Earth's mantle, *J. Geophys. Res.*, *81*(11), 1839–1846, doi:10.1029/JB081i011p01839.
Phipps Morgan, J., J. Hasenclever, M. Hort, L. Rüpke, and E. M. Parmentier (2007), On subducting slab entrainment of buoyant asthenosphere, *Terra Nova*, *19*, 167–173.
Press, W. H., S. A. Teukolsky, W. T. Vetterling, and B. P. Flannery (2007), *Numerical Recipes, 3rd Edition: The Art of Scientific Computing*, Cambridge Univ. Press, New York.
Ribe, N. M. (1992), On the relation between seismic anisotropy and finite strain, *J. Geophys. Res.*, *97*, 8737–8747, doi:10.1029/92JB00551.
Rodríguez-González, J., M. I. Billen, and A. M. Negredo (2014), Non-steady-state subduction and trench-parallel flow induced by overriding plate structure, *Earth Planet. Sci. Lett.*, *401*, 227–235.
Russo, R., and P. Silver (1994), Trench-parallel flow beneath the Nazca Plate from seismic anisotropy, *Science*, *263*, 1105–1111, doi:10.1126/science.263.5150.1105.
Schellart, W. P., D. R. Stegman, and J. Freeman (2008), Global trench migration velocities and slab migration induced upper mantle volume fluxes: Constraints to find an Earth reference frame based on minimizing viscous dissipation, *Earth Sci. Rev.*, *88*, 118–144, doi:10.1016/j.earscirev.2008.01.005.
Schmerr, N. (2012), The Gutenberg discontinuity: Melt at the lithosphere-asthenosphere boundary, *Science*, *335*, 1480–1483, doi:10.1126/science.1215433.
Skemer, P., J. M. Warren, and G. Hirth (2012), The influence of deformation history on the interpretation of seismic anisotropy, *Geochem. Geophys. Geosyst.*, *13*, Q03006, doi:10.1029/2011GC003988.
Song, T. R. A., and H. Kawakatsu (2012), Subduction of oceanic asthenosphere: Evidence from sub-slab seismic anisotropy, *Geophys. Res. Lett.*, *39*, L17301, doi:10.1029/2012GL052639.
Tovish, A., G. Schubert, and B. P. Luyendyk (1978), Mantle flow pressure and the angle of subduction: Non-Newtonian corner flows, *J. Geophys. Res.*, *83*, 5892–5898, doi:10.1029/JB083iB12p05892.
van Keken, P. E., et al. (2008), A community benchmark for subduction zone modeling, *Phys. Earth Planet. Inter.*, *171*, 187–197, doi:10.1016/j.pepi.2008.04.015.
Wada, I., and K. Wang (2009), Common depth of slab-mantle decoupling: Reconciling diversity and uniformity of subduction zones, *Geochem. Geophys. Geosyst.*, *10*, Q10009, doi:10.1029/2009GC002570.